INTERNATIONAL JOURNAL FOR NUMERICAL METHODS IN FLUIDS
Int. J. Numer. Meth. Fluids 2007; **55**:673–692
Published online 17 April 2007 in Wiley InterScience (www.interscience.wiley.com). DOI: 10.1002/fld.1489

Lattice Boltzmann methods for shallow water flow applications

Guido Thömmes[1], Mohammed Seaïd[2] and Mapundi K. Banda[3,*,†]

[1]*Fraunhofer Institut für Techno- und Wirtschaftsmathematik, Kaiserslautern 67663, Germany*
[2]*Fachbereich Mathematik, Universität Kaiserslautern, Kaiserslautern 67663, Germany*
[3]*School of Mathematical Sciences, University of KwaZulu-Natal, Scottsville 3209, South Africa*

SUMMARY

We apply the lattice Boltzmann (LB) method for solving the shallow water equations with source terms such as the bed slope and bed friction. Our aim is to use a simple and accurate representation of the source terms in order to simulate practical shallow water flows without relying on upwind discretization or Riemann problem solvers. We validate the algorithm on problems where analytical solutions are available. The numerical results are in good agreement with analytical solutions. Furthermore, we test the method on a practical problem by simulating mean flow in the Strait of Gibraltar. The main focus is to examine the performance of the LB method for complex geometries with irregular bathymetry. The results demonstrate its ability to capture the main flow features. Copyright © 2007 John Wiley & Sons, Ltd.

Received 17 December 2006; Revised 16 February 2007; Accepted 17 February 2007

KEY WORDS: shallow water equations; lattice Boltzmann method; Strait of Gibraltar

1. INTRODUCTION

The lattice Boltzmann (LB) method, also popularly referred to as LBM, is an alternative numerical tool for simulating fluid flows [1]. The method is based on statistical physics and models the fluid flow by tracking the evolution of distribution functions of the fluid particles in discrete phase space. The essential approach in the LB method lies in the recovery of macroscopic fluid flows from the microscopic flow behaviour of the particle movement or the mesoscopic evolution of particle distributions. The basic idea is to replace the nonlinear differential equations of macroscopic fluid dynamics by a simplified description modelled on the kinetic theory of gases. To obtain the hydrodynamic behaviour, the Chapman–Enskog expansion which exploits a small mean free path approximation to describe slowly varying solutions of the underlying kinetic equations is

*Correspondence to: Mapundi K. Banda, School of Mathematical Sciences, University of KwaZulu-Natal, Scottsville 3209, South Africa.
†E-mail: bandamk@ukzn.ac.za.

Contract/grant sponsor: Kaiserslautern University of Technology
Contract/grant sponsor: University of KwaZulu-Natal

undertaken. The method has been proven to be effective for simulating flows in complicated geometries and implementation on parallel computer architectures [2]. Furthermore, the method has become an alternative to other numerical methods like finite difference, finite element and finite volume methods in computational fluid dynamics.

As such the LB method has found a wide range of applications in a variety of fields, which include numerical simulation of shallow water equations. The LB method has been successfully adopted to simulate shallow water equations which describe wind-driven ocean circulation [3, 4], to model three-dimensional planetary geostrophic equations [5], and to study atmospheric circulation of the northern hemisphere with ideal boundary conditions [6]. In addition, under the influence of gravity, many free surface flows of a fluid (not necessarily involving water) can be modelled by the shallow water equations with the assumption that the vertical scale is much smaller than any typical horizontal scale. These equations can be derived from the depth-averaged incompressible Navier–Stokes equations and usually they include continuity and momentum equations. Hence, the applications of shallow water equations include a wide spectrum of phenomena other than water waves. For instance, the shallow water equations have been applied to environmental and hydraulic engineering, for example, for tidal flows in an estuary or coastal regions, rivers, reservoir, and open channel flows. Such practical flow problems are not trivial to simulate since the geometry can be complex and the topography irregular.

Other computational approaches such as the finite-difference method, the finite-volume method, or the finite-element method have been applied to simulate the shallow water equations, see [7–11] among others. For some of these approaches the treatment of bed slopes and friction forces often causes numerical difficulties in obtaining accurate solutions, see, for example, [7, 11, 12]. As an alternative, the LB method for shallow water equations has been presented in [3, 13, 14]. Due to its origin, the LB method has some features that are significantly different from conventional methods based on direct discretization of the equations. Appealing features of the LB method include simplicity in programming, parallel implementation, and straightforward incorporation of complex geometry and irregular topography. Furthermore, the LB method offers several desirable properties such as linear convection terms and nearest-neighbour stencils. On a structured mesh, the LB method can be implemented in a two-stage procedure namely, a collision operator evaluation which involves only local operations, and an advection operation where values are transported to adjacent lattice points without performing any computations.

In this paper, we mainly present a practical study of the LB method to shallow water problems on complex geometry and irregular bathymetry. The bathymetry is given either by an analytical function or by data points in a two-dimensional domain. The aim of this paper is to test the accuracy, efficiency, and study challenges for the LB approach for such a practical situation. To verify this approach, the problem of mean flow in the Strait of Gibraltar has been used as a test example. The results obtained are competitive in comparison with other approaches that solve the macroscopic equations using direct discretization methods. They are obtained without consideration for well balancing, or adaptive grids and other technical details as is the case with other approaches. By well-balanced schemes we mean those methods that require special treatment of the source terms such that the discretization of the flux gradients is balanced with the one used for the source terms. For more details on well-balanced schemes for shallow water equations we refer the reader to [11, 12, 15], while references on adaptive methods for solving shallow water equations can be found in [16] among others. Our findings inform applied scientists to consider the LB method as an alternative practical numerical scheme for solving flow problems modelled by the shallow water equations.

DOI: 10.1002/fld

The paper is organized as follows: in Section 2, we briefly describe the equations of shallow water flows; the LB method is formulated in Section 3; in Section 4, we examine the performance of the method for several test examples in one- and two-space dimensions. Conclusions are summarized in Section 5.

2. THE SHALLOW WATER EQUATIONS

In the current work, we formulate a LB method for the two-dimensional shallow water equations in the form

$$\begin{aligned}
&\partial_t h + \partial_x(hu_1) + \partial_y(hu_2) = 0 \\
&\partial_t(hu_1) + \partial_x\left(hu_1^2 + \frac{1}{2}gh^2\right) + \partial_y(hu_1u_2) = -gh\partial_x Z + \nabla\cdot(h\nu\nabla u_1) - \Omega u_2 - \frac{\tau_{\mathrm{b}_{u_1}}}{\rho} \\
&\partial_t(hu_2) + \partial_x(hu_1u_2) + \partial_y\left(hu_2^2 + \frac{1}{2}gh^2\right) = -gh\partial_y Z + \nabla\cdot(h\nu\nabla u_2) + \Omega u_1 - \frac{\tau_{\mathrm{b}_{u_2}}}{\rho}
\end{aligned} \tag{1}$$

where u_1 and u_2 are the depth-averaged flow velocities in the x- and y-directions, respectively, h the water depth, Z the bed elevation, g the gravitational acceleration, ρ the water density, Ω the Coriolis parameter defined by $\Omega = 2\omega\sin\phi$, with ω denoting the angular velocity of the Earth and ϕ is the geographical latitude. Furthermore, ν is the kinematic viscosity, and $\tau_{\mathrm{b}_{u_1}}$ and $\tau_{\mathrm{b}_{u_2}}$ denote the bed shear stress in the x- and y-directions, respectively, defined using the depth-averaged velocity as

$$\tau_{\mathrm{b}_{u_1}} = \rho C_{\mathrm{b}} u_1\sqrt{u_1^2+u_2^2}, \quad \tau_{\mathrm{b}_{u_2}} = \rho C_{\mathrm{b}} u_2\sqrt{u_1^2+u_2^2} \tag{2}$$

Here, C_{b} is the bed friction coefficient, which may be either constant or estimated from

$$C_{\mathrm{b}} = \frac{g}{C_z^2}$$

where $C_z = h^{1/6}/n_{\mathrm{b}}$ is the Chezy constant, and n_{b} denotes the Manning coefficient of the bed. In what follows, bold face types denote vector quantities and $\mathbf{u} = (u_1, u_2)^{\mathrm{T}}$ denotes the velocity field. The shallow water equations (1) have to be solved in a bounded spatial domain with smooth boundaries endowed with given initial and boundary conditions along with a prescribed bed elevation. In practice, these conditions are problem dependent and their discussion is postponed until Section 4 where numerical examples are discussed.

The treatment of topography and friction source terms is of major importance in many practical applications of shallow water models. Computational techniques using finite difference, finite element and finite-volume methods have been extensively studied in the literature. Furthermore, various numerical methods developed for general systems of hyperbolic conservation laws have been applied to the shallow water equations. For instance, most shock-capturing finite-volume schemes for shallow water equations are based on approximate Riemann solvers which were originally designed for hyperbolic systems without accounting for source terms such as bed slopes and friction losses. Therefore, most of these schemes suffer from numerical instability and may produce non-physical oscillations mainly because dicretizations of the flux and source terms are

DOI: 10.1002/fld

not well balanced in their reconstruction. The well-established Roe scheme [17] has been modified in [7] to treat source terms. This method was improved in [12] for general one-dimensional channel flows. However, for practical applications, this method may become computationally demanding due to its treatment of source terms. A Riemann solver inside a cell for balancing the source terms and the flux gradients has been proposed in [11]. However, the extension of this scheme to two-dimensional complex problems is not trivial. The performance of discontinuous Galerkin methods has been examined in [15] for some test examples on shallow water flows. A central-upwind scheme using the surface elevation instead of the water depth has been used in [18]. The ENO and WENO schemes have been extended in [19] to the one-dimensional shallow water equations. Numerical methods based on kinetic reconstructions have been studied in [20] for one-dimensional problems. In the framework of kinetic schemes, a class of relaxation methods has been proposed in [21]. Most of these methods require exact or approximate Riemann problem solvers, characteristic decompositions, reconstruction of numerical fluxes, and special discretization of the source terms which are not easy to implement for two-dimensional problems in complex geometry.

In the current work, we describe the application of an LB method for numerical solution of the two-dimensional shallow water equations. Results presented in this paper demonstrate reasonable resolution of the proposed method and confirm its capability to provide accurate and reliable simulations for shallow water type of flows which incorporate complex topography and friction forces.

3. THE LATTICE BOLTZMANN METHOD

We consider the two-dimensional kinetic equation

$$\frac{\partial f}{\partial t} + \mathbf{v} \cdot \nabla f = J(f) + S \tag{3}$$

which describes the evolution of a particle density $f(\mathbf{x}, \mathbf{v}, t)$ with $\mathbf{x} = (x, y)^{\mathrm{T}} \in \mathbb{R}^2$ and $\mathbf{v} = (v_1, v_2)^{\mathrm{T}} \in \mathbb{R}^2$. In (3), $\mathbf{v}$ is the microscopic velocity, J is the collision term, and S includes the effect of external forces. For discrete models in two-space dimensions, we assume

$$\mathbf{v} \in \{\mathbf{c}_0, \mathbf{c}_1, \ldots, \mathbf{c}_{N-1}\}$$

with $\mathbf{c}_i \in \mathbb{R}^2$. Here, we consider a D2Q9 square lattice model [22], as sketched in Figure 1, with velocity vector of particles defined by

$$\mathbf{c}_0 = \begin{pmatrix} 0 \\ 0 \end{pmatrix}, \quad \mathbf{c}_1 = \begin{pmatrix} 1 \\ 0 \end{pmatrix}, \quad \mathbf{c}_2 = \begin{pmatrix} 0 \\ 1 \end{pmatrix}, \quad \mathbf{c}_3 = \begin{pmatrix} -1 \\ 0 \end{pmatrix}, \quad \mathbf{c}_4 = \begin{pmatrix} 0 \\ -1 \end{pmatrix}$$

$$\mathbf{c}_5 = \begin{pmatrix} 1 \\ 1 \end{pmatrix}, \quad \mathbf{c}_6 = \begin{pmatrix} -1 \\ 1 \end{pmatrix}, \quad \mathbf{c}_7 = \begin{pmatrix} -1 \\ -1 \end{pmatrix}, \quad \mathbf{c}_8 = \begin{pmatrix} 1 \\ -1 \end{pmatrix}$$

In the discrete case, the $\mathbf{v}$-dependence of the particle distribution $f(\mathbf{x}, \mathbf{v}, t)$ is uniquely determined through N functions

$$f_i(\mathbf{x}, t) = f(\mathbf{x}, \mathbf{c}_i, t), \quad i = 0, 1, \ldots, N-1$$

DOI: 10.1002/fld

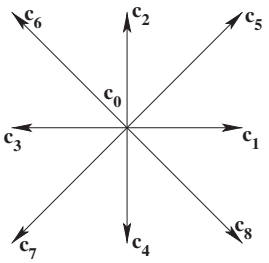

Figure 1. Links in the D2Q9 lattice Boltzmann method.

The physical variables, the water depth h, and the velocity $\mathbf{u}$, are defined in terms of the distribution functions as

$$h(\mathbf{x},t)=\sum_i f_i(\mathbf{x},t),\quad h\mathbf{u}=\sum_i \mathbf{c}_i f_i(\mathbf{x},t) \tag{4}$$

In most approaches for the LB applications, the collision operator $J(f)$ in (3) is typically of BGK-type [23]

$$J(f)=-\frac{1}{\tau}(f-f^{\mathrm{eq}}) \tag{5}$$

where the parameter $\tau>0$ is the relaxation time and f^{eq} is the equilibrium distribution depending on f *via* the variables h and $\mathbf{u}$ calculated according to (4). For the standard D2Q9 model with nine velocities applied to the shallow water equations, we have [3, 13]

$$f_i^{\mathrm{eq}}=\begin{cases} h-f_0^* h(\frac{15}{2}gh-\frac{3}{2}\mathbf{u}^2), & i=0,\\ f_i^* h(\frac{3}{2}gh+3\mathbf{c}_i\cdot\mathbf{u}+\frac{9}{2}(\mathbf{c}_i\cdot\mathbf{u})^2-\frac{3}{2}\mathbf{u}^2), & i=1,\ldots,8 \end{cases} \tag{6}$$

with the D2Q9 weight factors

$$f_i^*=\begin{cases} \frac{4}{9}, & i=0\\ \frac{1}{9}, & i=1,2,3,4\\ \frac{1}{36}, & i=5,6,7,8 \end{cases} \tag{7}$$

The local equilibrium function satisfies the following conditions:

$$\sum_i f_i^{\mathrm{eq}}=h,\quad \sum_i \mathbf{c}_i f_i^{\mathrm{eq}}=h\mathbf{u},\quad \sum_i \mathbf{c}_i\mathbf{c}_i f_i^{\mathrm{eq}}=\tfrac{1}{2}gh^2\mathbf{I}+h\mathbf{u}\otimes\mathbf{u} \tag{8}$$

such that the LB equation approaches the solution of the two-dimensional shallow water equations. In (8), $\mathbf{I}$ denotes the 2×2 identity matrix.

Hence, applying an explicit discretization of the above kinetic equation (3) with a BGK-type approximation (5), we obtain the following discrete LB equation:

$$f_i(\mathbf{x}+\mathbf{c}_i,t+1)-f_i(\mathbf{x},t)=-\frac{1}{\tau}(f_i-f_i^{\mathrm{eq}})+f_i^*\mathbf{c}_i\cdot\mathbf{F}(x,t) \tag{9}$$

DOI: 10.1002/fld

where $\mathbf{c}_i$ is the velocity vector of a particle on the ith link and $\mathbf{F}$ is the force vector

$$\mathbf{F}(\mathbf{x}, t) = \begin{pmatrix} -gh\partial_x Z - \Omega u_2 - \dfrac{\tau_{\mathrm{b}u_1}}{\rho} \\ -gh\partial_y Z + \Omega u_1 - \dfrac{\tau_{\mathrm{b}u_2}}{\rho} \end{pmatrix}. \tag{10}$$

By applying the Chapman–Enskog procedure [3], it can be shown that the solution of the LB equation with the equilibrium function (6) results in the solution of the shallow water equations (1) with a LB viscosity $\hat{\nu}$ defined as

$$\hat{\nu} = \tfrac{1}{6}(2\tau - 1) \tag{11}$$

In the presentation of the method above it is assumed for simplicity that the computational domain is discretized using a D2Q9 square lattice with unit spacing as shown in Figure 1. To match this discretization, the original shallow water equations are scaled in such a way that the lattice link is the reference length Δx. The time scale Δt should be chosen such that the ratio $U/c \ll 1$ is small enough to define a stable LB scheme. Here, $c = \Delta x/\Delta t$ denotes the velocity along a unit link and U is the typical velocity of the flow. This lattice viscosity is then related to the kinematic viscosity in (1) by the relation

$$\nu = c^2 \Delta t \hat{\nu} \tag{12}$$

In summary, the procedure to advance the solution from the time t_n to the next time t_{n+1} can be carried out in the following steps:

Step 1: Using the water depth and velocity at time t_n, compute the equilibrium function f_i^{eq}, $i = 0, 1, \ldots, 8$, from (6) to (7). Perform the collision step (5) to obtain the distributions f_i, $i = 0, 1, \ldots, 8$, with an appropriate relaxation time τ.

Step 2: Advect the distribution functions according to (9) and impose the corresponding boundary conditions.

Step 3: Update the water depth and velocity using Equations (4).

Step 4: Change the time $t_n \longrightarrow t_{n+1}$, go to Step 1 and repeat until a stopping criterion is fulfilled.

Note that the stopping criterion in Step 4 can be given either by a fixed time for unsteady problems, or by comparing the deviation between two consecutive solutions to test for convergence when simulating steady problems. Note that, although we have restricted our study to the D2Q9 square lattice, the presented LB method can also use the well-known seven-speed hexagonal lattice. The implementation of the LB method for this type of lattices can be carried out using similar formalism.

3.1. Boundary conditions

Boundary conditions play an important role in the LB method since they can influence the accuracy and stability of the LB method, compare [24, 25] for more discussions. When no-slip boundary conditions are imposed at walls the bounce-back rule is usually used in the LB algorithm. At a boundary point x_{b}, populations f_i of links c_i which intersect the boundary and point out of the fluid domain are simply reflected (bounce-back) since they cannot participate in the normal propagation step

$$f_{i*}(\mathbf{x}_{\mathrm{b}}, t+1) = f_i(\mathbf{x}_{\mathrm{b}}, t), \quad \mathbf{c}_{i*} = -\mathbf{c}_i$$

We use no-slip boundary conditions also for the coastlines in the Strait of Gibraltar (see Section 4.3).

DOI: 10.1002/fld

Boundary conditions in LB methods can also be realized by employing extrapolation rules using the equilibrium distribution. For the numerical examples considered in the present study, flow boundary conditions for the height, h, and/or the velocities, (u_1, u_2), are needed at the inlet and the outlet of computational domains. When the height h_l is prescribed at the left boundary, the three distributions f_1, f_5, and f_8 are unknown. We use the techniques described in [14, 24] for flat interfaces to implement these boundary conditions in the framework of the LB method.

Assuming that $u_2 = 0$, the velocity in x-direction can be recovered from the relation

$$h_l u_1 = h_l - (f_0 + f_2 + f_4 + 2(f_3 + f_6 + f_7))$$

and we define the unknown distributions as

$$\begin{aligned} f_1 &= f_3 + \tfrac{2}{3} h_l u_1 \\ f_5 &= f_7 - \tfrac{1}{2}(f_2 - f_4) + \tfrac{1}{6} h_l u_1 \\ f_8 &= f_6 + \tfrac{1}{2}(f_2 - f_4) + \tfrac{1}{6} h_l u_1 \end{aligned} \tag{13}$$

This method can also be used when the discharge $q_1 = hu_1$ is given since only the product of h and u_1 appears in Equations (13).

In the case of the Strait of Gibraltar we have both a boundary condition for the height and a Neumann boundary condition for the velocity for an inclined strait inlet and outlet. This class of boundary conditions is implemented by imposing the equilibrium distribution corresponding to the prescribed height, h_l, and the velocity of the nearest neighbour in the direction of the normal (u_{1n}, u_{2n})

$$f_i = f_i^{\mathrm{eq}}(h_l, u_{1n}, u_{2n}), \quad i = 0, 1 \ldots, 8$$

Other types of boundary conditions can also be incorporated. For more details on implementation of boundary conditions in LB methods, we refer to [24, 25] and further references therein.

4. NUMERICAL RESULTS

In this section, we examine the performance of the LB method in solving some well-established problems of shallow water flows. Three test examples are selected to check the accuracy and performance of the proposed LB approach. The first and second examples are one-dimensional problems with known analytical solutions and, therefore, are used to assess different features of the LB scheme such as accuracy in smooth regions and resolution in a non-flat topography. In the third example, we verify the capability of the LB method in a more complex fully two-dimensional problem. We apply the LB method to the problem of mean flow in the Strait of Gibraltar. In all the results presented in this section, the gravitational acceleration is fixed to $g = 9.81\ \mathrm{m/s^2}$.

4.1. Tidal wave flow

First, we consider the problem of a tidal wave flow in a frictionless ($C_b = 0$) channel with length, $L = 14$ km. The bottom is analytically defined by

$$Z(x) = 10 + \frac{40x}{L} + 10 \sin\left(\pi\left(\frac{4x}{L} - \frac{1}{2}\right)\right)$$

DOI: 10.1002/fld

The initial conditions for the water height and velocity are

$$h(x,0) = 60.5 - Z(x), \quad u(x,0) = 0$$

At the channel inflow and outflow, respectively, we prescribe

$$h(0,t) = 64.5 - 4\sin\left(\pi\left(\frac{4t}{86\,400} + \frac{1}{2}\right)\right), \quad u_1(L,t) = 0$$

Following [7], an asymptotic analytical solution for this example can be developed as

$$h(x,t) = 64.5 - Z(x) - 4\sin\left(\pi\left(\frac{4t}{86\,400} + \frac{1}{2}\right)\right)$$

$$u_1(x,t) = \frac{(x-L)\pi}{5400h(x,t)}\cos\left(\pi\left(\frac{4t}{86\,400} + \frac{1}{2}\right)\right)$$

This asymptotic analytical solution is used to quantify the results obtained by the LB method. We define the relative L^∞-, L^1- and L^2-error norms as

$$\|\mathbf{e}\|_{L^\infty} = \frac{\max_{ij}|e_{ij}^n|}{\max_{ij}|u_{ij}^n|}, \quad \|\mathbf{e}\|_{L^1} = \frac{\sum_{ij}|e_{ij}^n|}{\sum_{ij}|u_{ij}^n|}, \quad \|\mathbf{e}\|_{L^2} = \frac{\sqrt{\sum_{ij}|e_{ij}^n|^2}}{\sqrt{\sum_{ij}|u_{ij}^n|^2}}$$

where $e_{ij}^n = u_{ij}^n - u(x_i, y_j, t_n)$ is the error between the numerical solution, u_{ij}^n, and the analytical solution, $u(x_i, y_j, t_n)$, at time t_n and lattice point (x_i, y_j). Here, the subscript for the x-direction has been ignored to avoid overcrowding the variables with subscripts. For the LB method, we used $\tau = 0.6$, $c = 200$ m/s and the results are displayed at time $t = 9117.5$ s. For this test example the ratio is $U/c = 0.0009$. Note that we used a two-dimensional code to reproduce numerical solutions for the one-dimensional problem. Therefore, boundary conditions in the y-direction have to be supplied for the two-dimensional code. For this test example, the dimension in y-direction is fixed to 50 lattice points. Periodic boundary conditions are assumed on the upper and lower walls.

In Figure 2, we plot the error norms for the velocity solution using four uniform lattices with sizes $\Delta x = \Delta y = 56$, 28, 14 and 7 m. Logarithmic scales are used on the x- and y-axes. It is easy to verify that decreasing the lattice size results in a decrease of all error norms. Similar behaviour has been observed for the water depth. As expected the LB method shows a first-order accuracy for this test example. The velocity values corresponding to the considered lattices are plotted along the analytical solution as shown in Figure 3. Grid convergence is clearly observed in this figure. Only a small difference between the LB solutions obtained with lattice resolution $\Delta x = \Delta y = 7$ m and the asymptotic analytical solution is observed.

Figure 4 presents the numerical and analytical solutions for the free surface at the simulation time $t = 9117.5$ s using $\Delta x = \Delta y = 7$ m. There is an excellent agreement between the numerical results obtained by the LB method and the asymptotic analytical solution. The LB method performs well for this unsteady test example and produces accurate solutions without requiring special treatment of the source terms or complicated upwind discretization of the gradient fluxes as in [7] among others.

DOI: 10.1002/fld

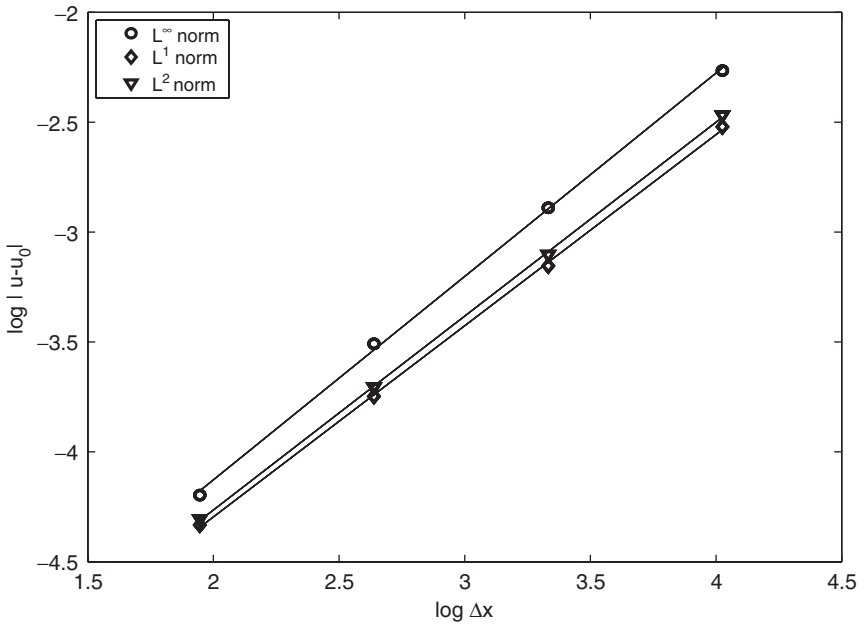

Figure 2. Grid convergence for the tidal wave flow at time $t = 9117.5$ s.

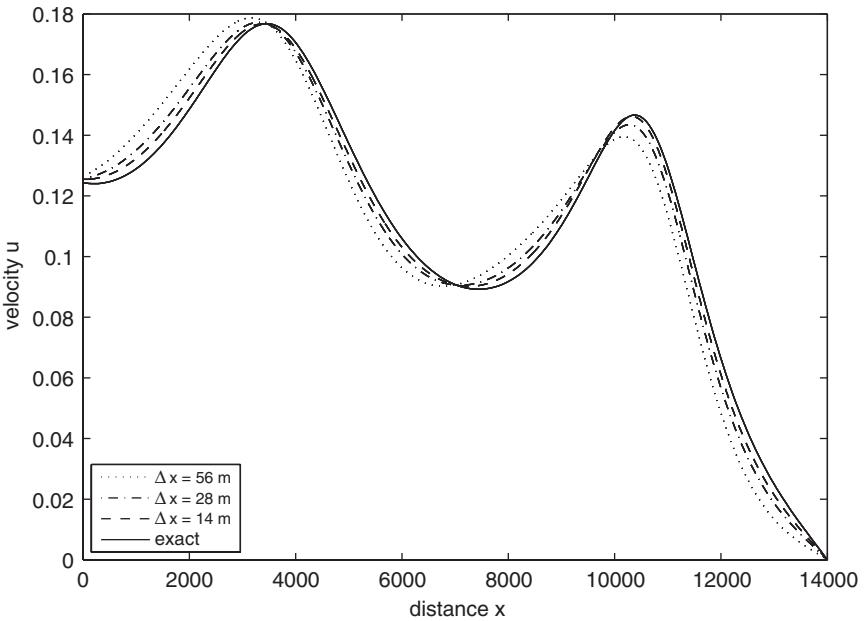

Figure 3. Velocity plots for the tidal wave flow on different meshes at time $t = 9117.5$ s.

DOI: 10.1002/fld

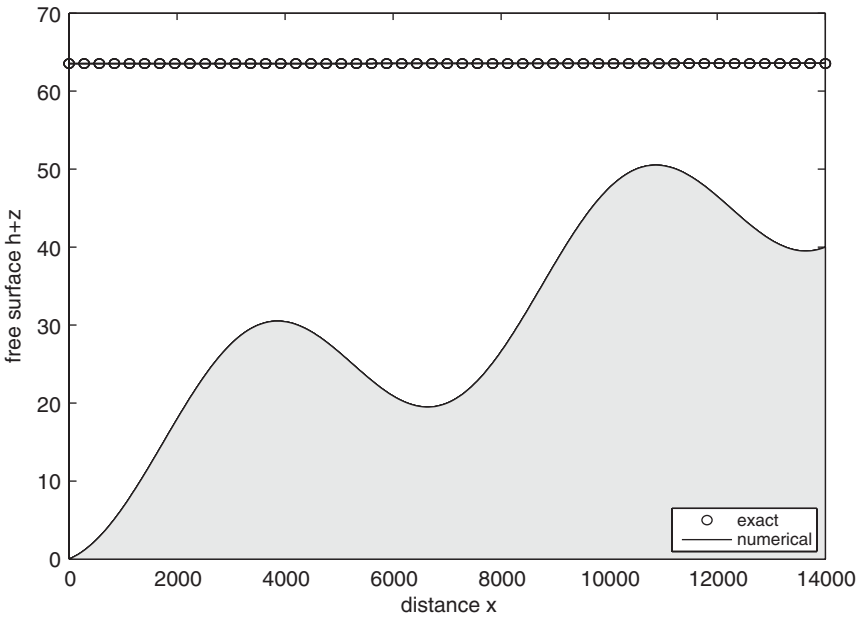

Figure 4. Numerical and analytical free surface for the tidal wave flow at time $t = 9117.5$ s.

4.2. *Steady flow over a hump*

Next, we consider the benchmark problem of steady flow over a hump studied in [12] among others. The emphasis is to investigate the ability of the LB method to recover the correct steady-state solution for shallow water flows on non-flat topography. In this test example, the channel length is 25 m and the bottom topography is defined as

$$Z(x) = \begin{cases} 0.2\text{ m} - 0.05\text{ m}^{-1}\ (x - 10\text{ m})^2 & \text{if } 8\text{ m} \leqslant x \leqslant 12\text{ m} \\ 0\text{ m} & \text{otherwise} \end{cases} \tag{14}$$

The initial conditions are given by

$$h(x, 0) = 2\text{ m} - Z(x), \quad u_1(x, 0) = 0\text{ m/s} \tag{15}$$

On the channel boundaries we use an inflow boundary condition for the discharge $q = hu_1 = 4.42\text{ m}^2/\text{s}$ and an outflow condition for the height $h = 2$ m.

For this test example, we have observed that the large value of the discharge causes instabilities which could be controlled by introducing an initialization phase where we continuously increase the discharge until it reaches its final value. The transition was done over the first half of the simulation time using a $C^2(\mathbb{R})$ (twice continuously differentiable) function as

$$\varphi(\xi) = \begin{cases} 0 & \text{if } \xi \leqslant 0 \\ 1 & \text{if } \xi \geqslant 1 \\ \xi^3(10 - 15\xi + 6\xi^2) & \text{otherwise} \end{cases} \tag{16}$$

DOI: 10.1002/fld

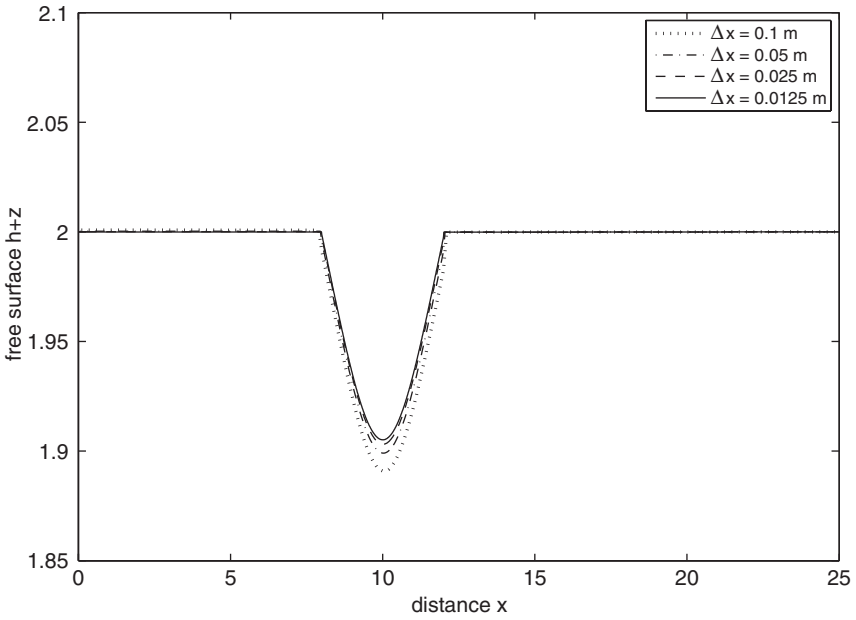

Figure 5. Water free surface for the steady flow over a hump using four different lattices.

Thus, the modified discharge $\tilde{q}$ is set over the course of the simulation

$$\tilde{q}(t) = \varphi\left(\frac{t}{T_{\text{init}}}\right) q$$

where the initialization time $T_{\text{init}} = 250$ s. The y-dimension of the channel was set to 50 lattice points. Periodic boundary conditions were imposed on the upper and lower boundary walls. We used $c = 15\text{m/s}$, $\tau = 1.5$ and simulations were stopped at time $t = 500\text{s}$. At this time, the flow had all the characteristic features of the steady-state solution. In this example, the ratio was $U/c = 0.133$.

Lattice convergence was also investigated for this test problem. We consider four uniform lattices with sizes $\Delta x = 0.1, 0.05, 0.025$ and 0.0125 m. The results obtained for the free surface are depicted in Figure 5. Significant improvement is observed between the results obtained on the mesh with $\Delta x = 0.1$ m and the mesh with $\Delta x = 0.0125$ m. On the last two finest meshes the solutions appear to be lattice independent. Thus, the mesh with $\Delta x = 0.025$ m is considered for the next simulations of this test example.

Figure 6 shows the free surface along with the bottom profile. The water discharge and the pointwise errors in the discharge are presented in Figure 7. The LB method reproduces the correct steady flow and resolves this test problem accurately with small errors in the discharge plot over the hump area. These errors in the discharge are expected since the correct capturing of the water discharge is more difficult than the water height in this test case. The results shown here compare favourably with those published in the literature for the problem of steady flow over a hump, see for example, [11, 12]. Note that the performance of the LB approach is very attractive since the computed solutions remain stable and accurate even when coarse lattices are used without solving

DOI: 10.1002/fld

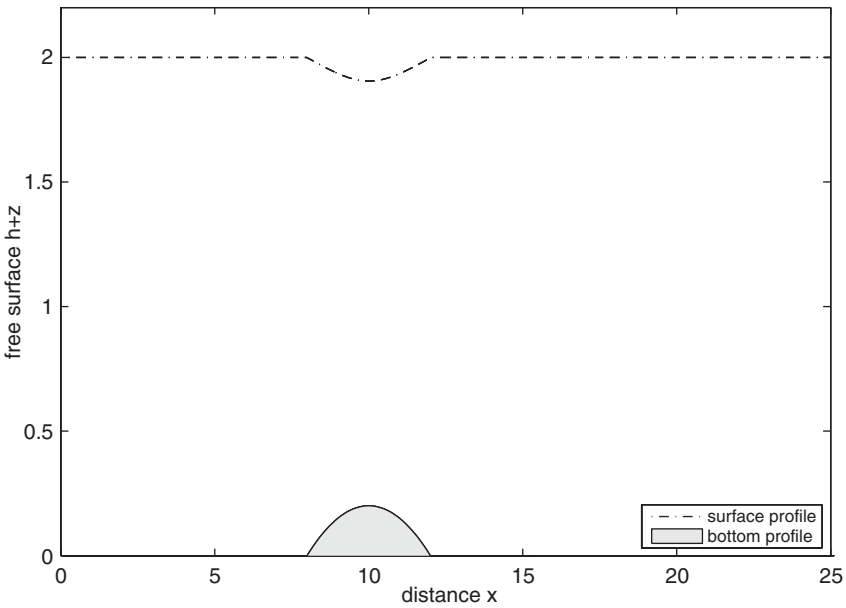

Figure 6. Water free surface and bottom bed for the steady flow over a hump.

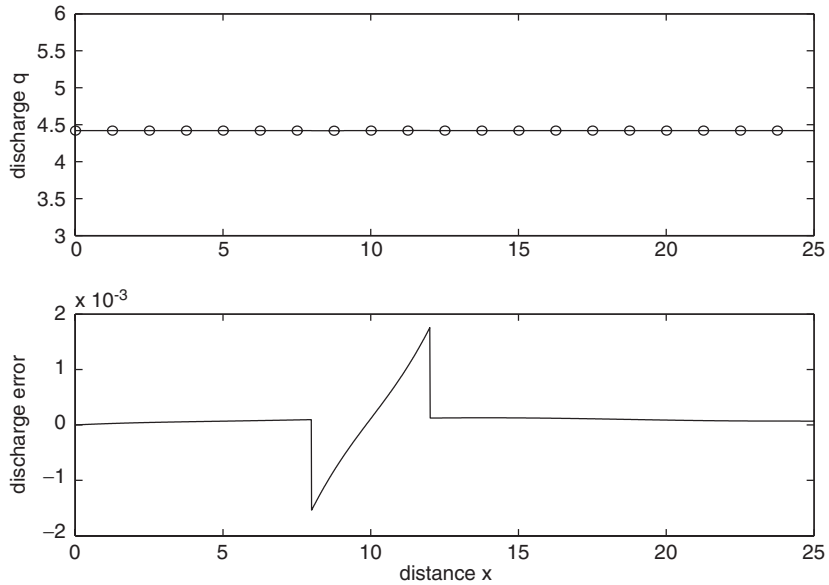

Figure 7. Water discharge (top) and discharge error (bottom) for the steady flow over a hump.

DOI: 10.1002/fld

Riemann problems or reconstructing upwind fluxes or requiring complicated techniques to balance the source terms and flux gradients as in [11, 12].

4.3. Mean flow in the Strait of Gibraltar

The final application is the problem of mean flow in the Strait of Gibraltar. The schematic description of the Strait of Gibraltar is given in Figure 8. The system is bounded to the north and south by the Iberian and African continental forelands, respectively, and to the west and east by the Atlantic ocean and the Mediterranean sea, respectively. This test problem is chosen because it presents a true practical test of LB shallow water flow for two major reasons. First, the Strait of Gibraltar's domain is a large-scale domain including high gradients of the bathymetry and well-defined shelf regions. Secondly, the strait contains complex fully two-dimensional flow structures, which present a challenge in the shallow water modelling. The Strait of Gibraltar has also been the subject of numerous investigations such as water circulation, hydrodynamic processes and tides, compare [26–29] among others. In all these references, the simulation domain is restricted by the Tangier–Barbate axis from the Atlantic ocean and the Ceuta–Algeciras axis from the Mediterranean sea, see Figure 9. This domain is taken in numerical simulations mainly because measured data are usually provided by stations located on the above-mentioned cities. Therefore, we have adapted the same domain for our LB simulations. Our main objective in this numerical example is to test the capability of the LB method to handle complex geometry and irregular topography.

The bathymetry of the strait is obtained from [27] and it is depicted in Figure 9. In this figure we show 10 equally spaced bathymetric contourlines. It is evident that the bathymetry is not smooth and exhibits irregular features with different length scales. For instance, two bumps with minimum bathymetric values of 997 and 463 m are localized in the vicinity of the eastern exit of the strait and the Caraminal Sill, respectively. All simulations used a constant Manning coefficient

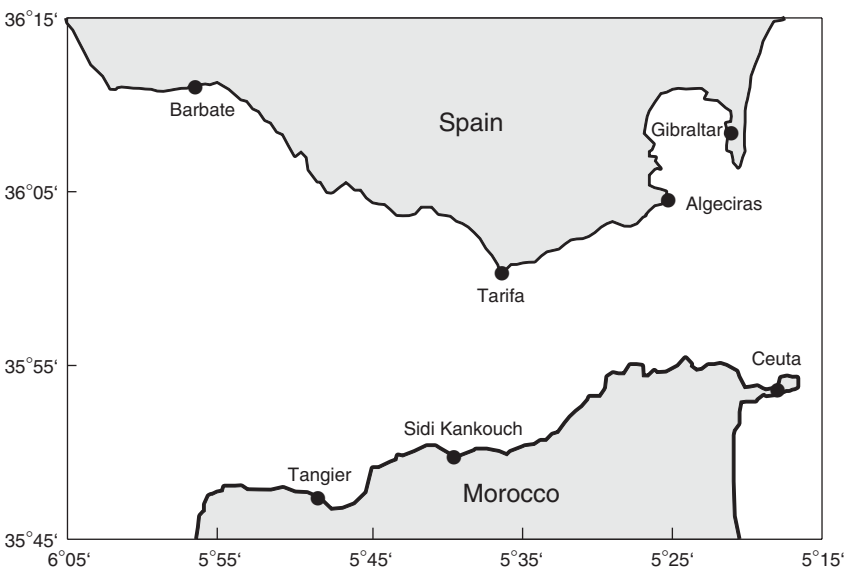

Figure 8. Schematic description of the Strait of Gibraltar.

DOI: 10.1002/fld

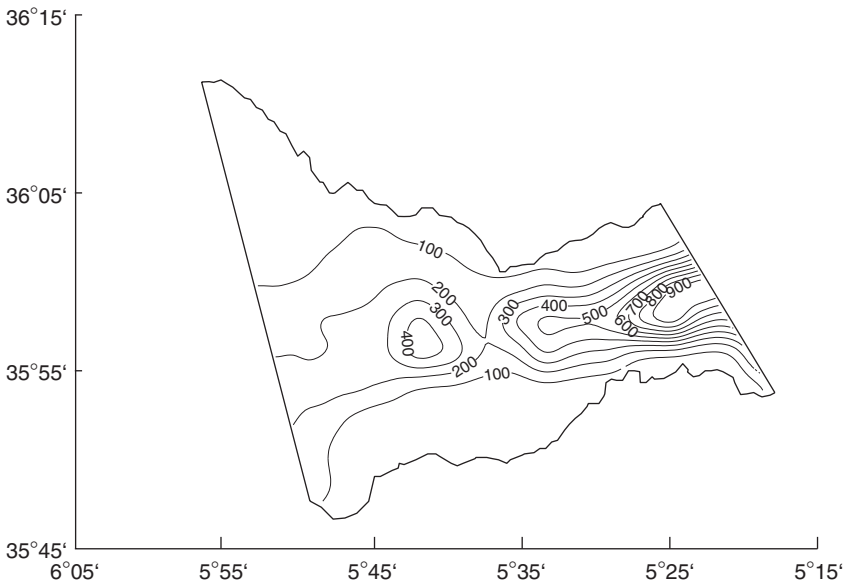

Figure 9. Bathymetry contours of the domain under study in the Strait of Gibraltar.

of $n_b = 0.012$ s/m$^{1/3}$, a Coriolis parameter of $\Omega = 8.55 \times 10^{-5}$ s^{-1}, and a typical value for the horizontal eddy viscosity of $\nu = 100$ m^2/s known in the literature, see, for example, [27, 29]. A no-slip boundary condition for velocity variables was applied to the coastal boundaries. At the open boundaries, Neumann boundary conditions are imposed for the velocity, and the water elevation is prescribed as a periodic function of time using the main semidiurnal and diurnal tides. The tidal constants at the open boundary lattice nodes were calculated by interpolation from those measured at the coastal stations Tangier and Barbate on the western end and the coastal stations Ceuta and Algeciras on the eastern end of the strait. We considered the main semidiurnal M_2, S_2, and N_2 tidal waves, and the diurnal K_1 tidal wave in the Strait of Gibraltar. Hence, at the open boundaries

$$h(x, y, t) = h_0 + h^*(x, y)e^{i(\omega^* t + \varphi^*)} \tag{17}$$

where the wave amplitude $h^*(x, y)$ is obtained by linear interpolation from given data for the considered tides at the Tangier and Barbate stations for the western open boundary and at the Ceuta and Algeciras stations for the eastern open boundary. In (17), h_0 is the averaged water elevation set to 3 m in our simulations, and ω^* and φ^* denote angular frequency and phase of the tide. Characteristic values for these parameters are taken from [27] and for completeness are listed in Table I. Initially, the flow was at rest and 2 weeks of real time were simulated. At the end of the simulation time the velocity fields were sampled for each tidal simulation at four different times $t = 0$, $T/4$, $T/2$ and $3T/4$, where T represents the period of the considered tidal wave.

First, we examined the lattice dependence of the solutions. To this end, we ran the LB code using the M_2 tidal conditions on three different meshes with lattice sizes $\Delta x = \Delta y = 500$, 250 and 125 m. In Figure 10, we show the cross-sections of the water height at mid-width of the strait at times $t = T/4$ and $3T/4$. It is evident that, for this flow regime, the results obtained on the coarse

DOI: 10.1002/fld

Table I. Tidal waves and reference parameters considered in the present study.

Station	Tide	h^* (m)	ω^* (rad/s)	φ^* (◦)
Tangier	M_2	0.680	1.4052×10^{-4}	−67.00
	S_2	0.250	1.4544×10^{-4}	−90.00
	N_2	0.130	1.3788×10^{-4}	−56.00
	K_1	0.060	7.2921×10^{-5}	−80.00
Barbate	M_2	0.762	1.4052×10^{-4}	−53.50
	S_2	0.279	1.4544×10^{-4}	−77.00
	N_2	0.160	1.3788×10^{-4}	−37.00
	K_1	0.027	7.2921×10^{-5}	−59.00
Ceuta	M_2	0.288	1.4052×10^{-4}	−55.02
	S_2	0.105	1.4544×10^{-4}	−76.13
	N_2	0.071	1.3788×10^{-4}	−37.38
	K_1	0.038	7.2921×10^{-5}	−147.72
Algeciras	M_2	0.323	1.4052×10^{-4}	−34.80
	S_2	0.121	1.4544×10^{-4}	−65.76
	N_2	0.075	1.3788×10^{-4}	−34.96
	K_1	0.025	7.2921×10^{-5}	−129.72

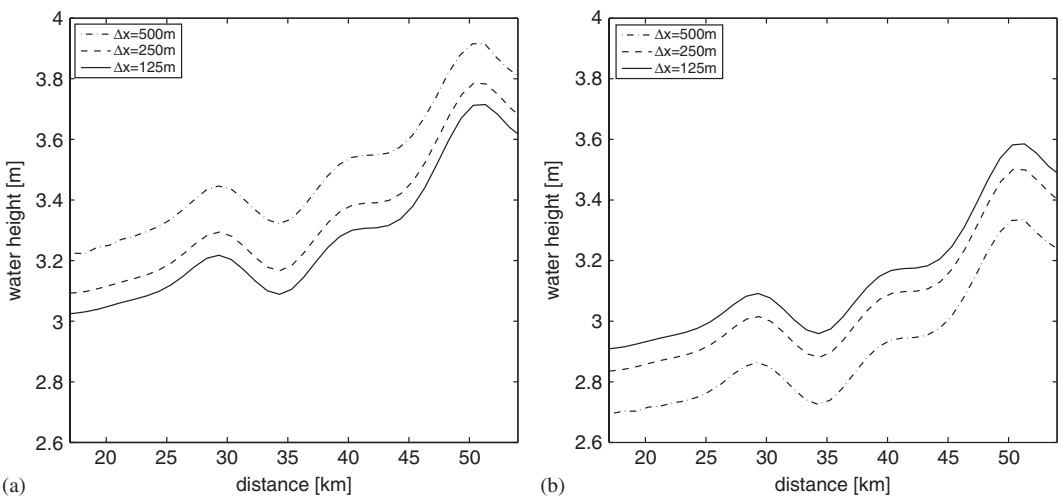

Figure 10. Water height using the M_2 tidal wave on different meshes: (a) $t = T/4$ and (b) $t = 3T/4$.

lattice of 500 m show differences to those obtained on the fine lattice of 125 m. These differences noticeably decrease for the lattice of 250 m. For instance, the discrepancies in the maximum water height on the lattices with sizes 250 and 125 m are less than 1.92 and 2.34% at $t = T/4$ and $3T/4$, respectively. Similar results, not reported here, were obtained for the water velocity and for the

DOI: 10.1002/fld

other tidal waves. Therefore, bearing in mind the relatively small differences on the results from a lattice with size 125 and 250 m at the expense of rather significant increase in the computational costs, the lattice with size 250 m was believed to be adequate to obtain reasonable results subject to minimal lattice effects. Hence, the results presented herein are based on the mesh with lattice size $\Delta x = \Delta y = 250$ m.

The computed velocity fields using the parameters of the semidiurnal M_2, S_2, and N_2 tidal waves are presented in Figures 11–13, respectively. The results for the diurnal K_1 tidal wave are presented in Figure 14. We display the results at four different times using the corresponding time period of each tide. Once the period is completed, dynamics of the water flow is repeated reproducing analogous velocity fields. The results show different aspects in the flow generated using tidal conditions for the semidiurnal M_2, S_2, and N_2 tidal waves and those obtained using the diurnal K_1 tidal wave. Using the conditions for the semidiurnal tides, the flow exhibits a recirculating zone of different magnitudes near the Craminal Sill. At later time, before the period is completed, the flow generated by semidiurnal M_2, S_2, and N_2 tidal waves changes the direction pointing towards the Atlantic ocean. This behaviour was not observed in the flow field obtained using conditions of the diurnal K_1 tidal wave. In this latter test case, the flow shows slow dynamics and does not change the direction during the simulation time. A recirculating flow region is also detected on the top-eastern exits of the strait near Algeciras. Similar features have also been reported in [26, 27]. The LB shallow water model performs well for this test problem since it does not diffuse the moving fronts and no spurious oscillations have been observed near steep gradients of the flow field in the computational domain. It can be clearly seen that the complicated flow structures on the Caraminal Sill and near Tarifa narrows and Tangier basin are being captured by the LB method. In addition, the presented results clearly indicate that the method is suitable for the prediction of mean flow in the Strait of Gibraltar.

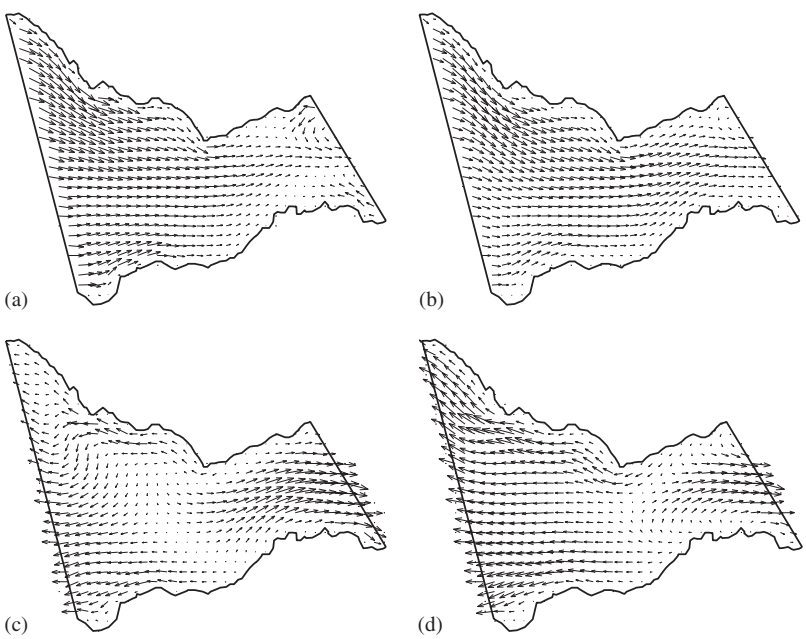

Figure 11. Results using the M_2 tidal wave: (a) $t = 0$; (b) $t = T/4$; (c) $t = T/2$; and (d) $t = 3T/4$.

DOI: 10.1002/fld

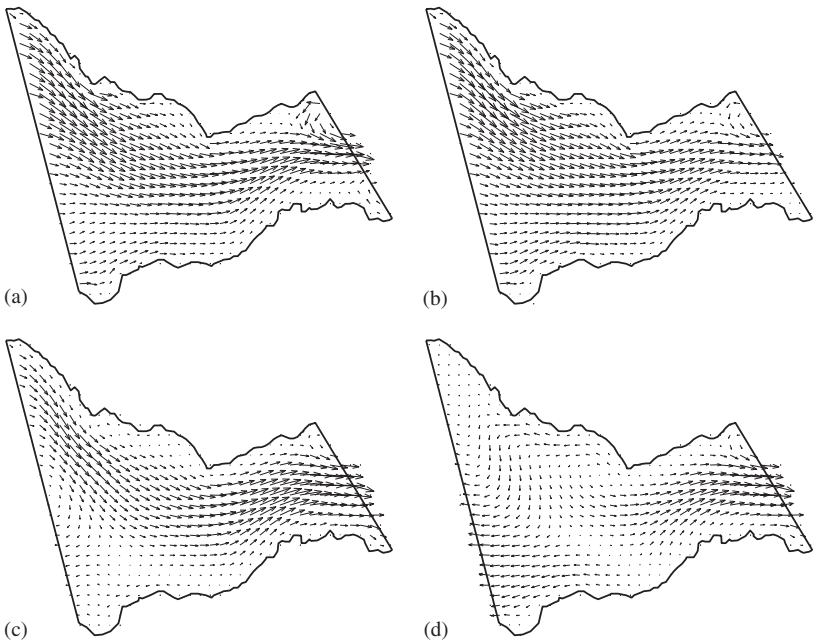

Figure 12. Results using the S_2 tidal wave: (a) $t=0$; (b) $t=T/4$; (c) $t=T/2$; and (d) $t=3T/4$.

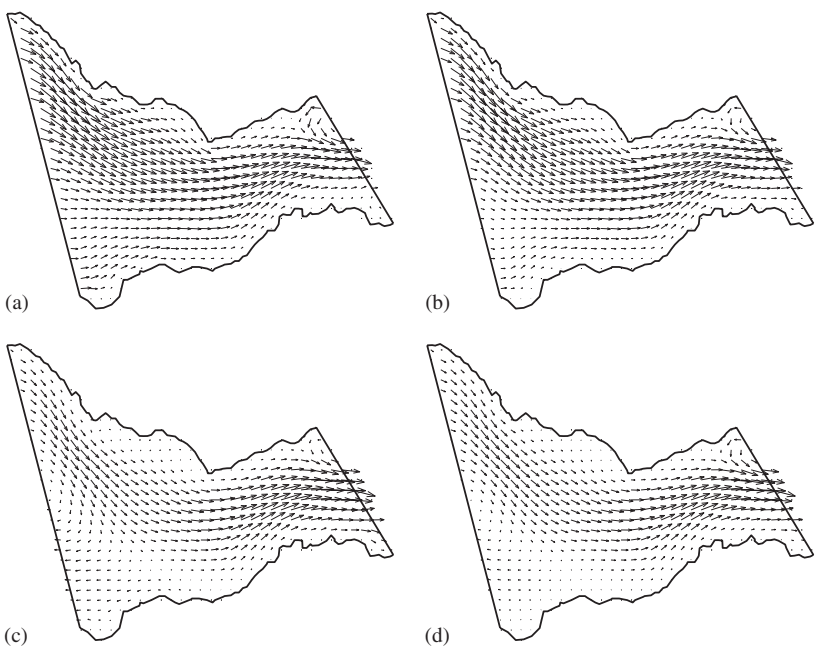

Figure 13. Results using the N_2 tidal wave: (a) $t=0$; (b) $t=T/4$; (c) $t=T/2$; and (d) $t=3T/4$.

DOI: 10.1002/fld

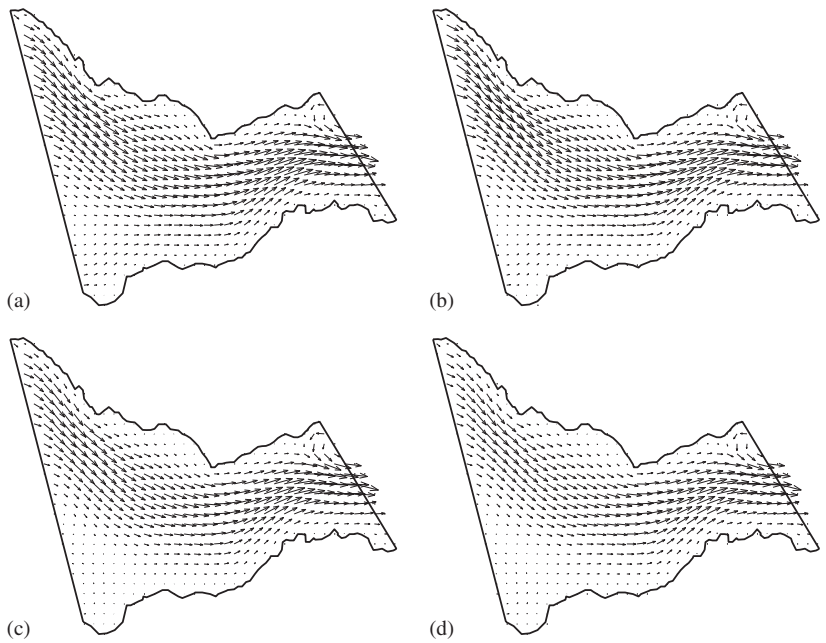

Figure 14. Results using the K_1 tidal wave: (a) $t=0$; (b) $t=T/4$; (c) $t=T/2$; and (d) $t=3T/4$.

Finally, computational cost, in terms of CPU seconds per time step, is 0.22 s for each simulation using the M_2, S_2, N_2, and K_1 tidal waves. Approximately 2×10^6 time steps were needed to reach the real time of 2 weeks in a solution. All the computations were performed on a Pentium IV 2.66 GHz having 1 Gb of RAM. Considering the computational cost and the accuracy achieved, the LB algorithm can be considered as a competitive alternative to the finite volume methods widely used in the literature to perform numerical studies on shallow water flows, in terms of both numerical accuracy and computational cost.

This is an important result when it comes to numerically efficient tools in shallow water simulations; given that the LB model is significantly simpler than the finite volume or finite element methods with regard to mathematical details and implementation effort. It should be noted that the LB method offers significant convenience for practical applications, that it can be easily incorporated in a shallow water analysis by simply introducing an equilibrium function and forces describing the mean flow variables and the bathymetric effects. Moreover, since the LB method is well suited for parallel computing, the CPU time of the scheme can be drastically reduced if parallel computers are used.

5. CONCLUSIONS

The most common two-dimensional LB method using nine particle speeds arranged on a D2Q9 squared lattice was used to approximate numerical solutions to the shallow water equations. The model is simple, accurate, easy to implement, and can be used to solve both steady and unsteady shallow water problems. The method also provides a straightforward treatment of source terms

DOI: 10.1002/fld

without relying on complicated discretization techniques. Other source terms such as wind stresses or bed shear stresses can naturally be added to the LB equation as force terms without special treatment. In this paper, our focus is to demonstrate the ability of the LB method to solve practical shallow water flows on non-flat beds with irregular bathymetry.

The efficiency of the method for predicting shallow water flows was assessed in the benchmark problems of tidal wave flow and steady flow over a hump. The results clearly indicate that the method captures the correct flow structures and reproduces results which satisfactorily agree with those available in the literature for the same test problems. To demonstrate the ability of the LB method on complex practical shallow water problems, we have applied the method to the mean flow in the Strait of Gibraltar. The numerical results show correct physics in different test regimes. The influence of different spatial resolutions on the numerical results has also been discussed. Refined spatial models in which a larger number of total particles is used in the simulation can resolve more small-scale effects at the expense of long computational times. Nevertheless, flows in such complex domains can be computed, providing correct physics without the need for generating adaptive grids or complicated reconstruction of numerical fluxes using exact or approximate Riemann solvers. Overall the method shows reasonable accuracy while ensuring the required properties of the shallow water flows.

ACKNOWLEDGEMENTS

M. K. Banda acknowledges the support from the Excellence Cluster 'Dependable Adaptive Systems and Mathematical Modelling' at the Kaiserslautern University of Technology and the Competitive Research Grant (2006) 'Flow Models with Source Terms, Scientific Computing, Optimisation in Applications' of the University of KwaZulu-Natal for his visit to Technomathematics Group at Kaiserslautern University during which part of this work was undertaken.

REFERENCES

1. Chen S, Doolen GD. Lattice Boltzmann method for fluid flows. *Annual Review of Fluid Mechanics* 1998; **30**:329–364.
2. Kandhai D, Koponen A, Hoekstra AG, Kataja M, Timonen J, Sloot PMA. Lattice Boltzmann hydrodynamics on parallel systems. *Computer Physics Communications* 1998; **111**:14–26.
3. Salmon R. The lattice Boltzmann method as a basis for ocean circulation modeling. *Journal of Marine Research* 1999; **57**:503–535.
4. Zhong L, Feng S, Gao S. Wind-driven ocean circulation in shallow water lattice Boltzmann model. *Advances in Atmospheric Sciences* 2005; **22**:349–358.
5. Salmon R. The lattice Boltzmann solutions of the three-dimensional planetary geostrophic equations. *Journal of Marine Research* 1999; **57**:847–884.
6. Feng S, Zhao Y, Tsutahara M, Ji Z. Lattice Boltzmann model in rotational flow field. *Chinese Journal of Geophysics* 2002; **45**:170–175.
7. Bermúdez A, Vázquez ME. Upwind methods for hyperbolic conservation laws with source terms. *Computers and Fluids* 1994; **23**:1049–1071.
8. Zhou JG. Velocity–depth coupling in shallow water flows. *Journal of Hydrologic Engineering* (ASCE) 1995; **10**:717–724.
9. Stansby PK, Zhou JG. Shallow water flow solver with non-hydrostatic pressure: 2D vertical plane problems. *International Journal for Numerical Methods in Fluids* 1998; **28**:541–563.
10. Toro EF. Riemann problems and the WAF method for solving two-dimensional shallow water equations. *Philosophical Transactions of the Royal Society of London, Series A* 1992; **338**:43–68.
11. LeVeque RJ. Balancing source terms and the flux gradients in high-resolution Godunov methods: the quasi-steady wave-propagation algorithm. *Journal of Computational Physics* 1998; **146**:346–365.

DOI: 10.1002/fld

12. Vázquez-Cendón ME. Improved treatment of source terms in upwind schemes for shallow water equations in channels with irregular geometry. *Journal of Computational Physics* 1999; **148**:497–526.
13. Dellar PJ. Non-hydrodynamic modes and a priori construction of shallow water lattice Boltzmann equations. *Physical Review E* (*Statistical Nonlinear Soft and Matter Physics*) 2002; **65**:036309.
14. Zhou JG. A lattice Boltzmann model for the shallow water equations. *Computer Methods in Applied Mechanics and Engineering* 2002; **191**:3527–3539.
15. Xing Y, Shu C. High order well-balanced finite volume WENO schemes and discontinuous Galerkin methods for a class of hyperbolic systems with source terms. *Journal of Computational Physics* 2006; **214**:567–598.
16. Marrocu M, Ambrosi D. Mesh adaptation strategies for shallow water flow. *International Journal for Numerical Methods in Fluids* 1999; **31**:497–512.
17. Roe PL. Approximate Riemann solvers, parameter vectors and difference schemes. *Journal of Computational Physics* 1981; **43**:357–372.
18. Kurganov A, Levy D. Central-upwind schemes for the Saint-Venant system. *Mathematical Modelling and Numerical Analysis* 2002; **36**:397–425.
19. Vukovic S, Sopta L. ENO and WENO schemes with the exact conservation property for one-dimensional shallow-water equations. *Journal of Computational Physics* 2002; **179**:593–621.
20. Perthame B, Simeoni C. A kinetic scheme for the Saint-Venant system with a source term. *CALCOLO* 2001; **38**:201–231.
21. Seaïd M. Non-oscillatory relaxation methods for the shallow water equations in one and two space dimensions. *International Journal for Numerical Methods in Fluids* 2004; **46**:457–484.
22. Qian YH, d'Humieres D, Lallemand P. Lattice BGK models for the Navier–Stokes equation. *Europhysics Letters* 1992; **17**:479–484.
23. Bhatnagar P, Gross E, Krook M. A model for collision process in gases. *Physical Review Letters* 1954; **94**:511–525.
24. Zou Q, He X. On pressure and velocity boundary condition for the lattice Boltzmann BGK model. *Physics of Fluids* 2002; **9**(6):1591–1598.
25. Gallivan MA, Noble DR, Georgiads JG, Buckius RO. An evaluation of the bounce-back boundary condition for lattice Boltzmann simulations. *International Journal for Numerical Methods in Fluids* 1997; **25**:249–263.
26. Almazán JI, Bryden H, Kinder T, Parrilla G (eds). *Seminario Sobre la Oceanografía Física del Estrecho de Gibraltar*. SECEG: Madrid, 1988.
27. González M, Sánchez-Arcilla A. Un Modelo Numérico en Elementos Finitos para la Corriente Inducida por la Marea. Aplicaciones al Estrecho de Gibraltar. *Revista Internacional de Métodos Numéricos para Cálculo y Diseño en Ingeniería* 1995; **11**:383–400.
28. Lafuente JG, Almazán JL, Catillejo F, Khribeche A, Hakimi A. Sea level in the strait of Gibraltar: tides. *International Hydrographic Review LXVII* 1990; **1**:111–130.
29. Tejedor L, Izquierdo A, Kagan BA. Sein DV. Simulation of the semidiurnal tides in the strait of Gibraltar. *Journal of Geophysical Research* 1999; **104**:13541–13557.

DOI: 10.1002/fld